*Journal of Engineering Mathematics* **26**: 349–361, 1992.



# Inversion of the source and vorticity equations for supercavitating hydrofoils

SPYROS A. KINNAS

*Department of Ocean Engineering, Massachusetts Institute of Technology, Room 5-221, 77 Massachusetts Avenue, Cambridge, MA 02139, U.S.A.*

Received 19 March 1991; accepted in revised form 15 August 1991

**Abstract.** The problem of a supercavitating hydrofoil of general shape with leading edge cavity detachment is addressed in linear theory in terms of unknown source and vorticity distributions on the foil and cavity. The related singular integral equations are inverted analytically and the cavitation number, the source and vorticity distributions are expressed in terms of integrals of quantities which depend only on the hydrofoil shape and the cavity length. Numerical algorithms for computing these integrals accurately and efficiently are given.

## 1. Introduction

The analysis of the flow around a supercavitating hydrofoil is an essential tool in the overall design of high speed hydrofoil boats. It also constitutes the basis of more complicated flows such as those about supercavitating, ventilated or surface piercing propellers.

Linear theory was first applied by Tulin to the problem of supercavitating symmetric sections at zero incidence and zero cavitation number [1], then to the problem of general camber meanlines at zero cavitation number [2], and to a supercavitating flat plate at incidence and arbitrary cavitation numbers [3]. It was subsequently extended to supercavitating hydrofoils of general shape at non-zero cavitation numbers by Wu [4], Geurst [5], Parkin [6], Fabula [7], and Nishiyama and Ota [8]. The previous authors formulated the problem in terms of the complex perturbation velocity function, which was then determined from the application of the boundary condition on the foil, on the cavity, and at infinity.

Hanaoka [9] formulated the linearized partial and supercavitating hydrofoil problem in terms of the perturbation velocity potential which he expressed in terms of singularity distributions on the foil. He also gave series representations for the cavitation number, the hydrodynamic coefficients and the cavity shape when the hydrofoil shape could be expressed in terms of polynomials in the chordwise coordinate.

More recently, the non-linear flow around supercavitating hydrofoils has been addressed by employing numerical boundary element (panel) methods [10, 11, 12]. These methods discretize the hydrofoil and cavity surface into panels and apply the exact kinematic and dynamic boundary conditions on the exact cavity surface whose shape is determined iteratively. A drawback of the numerical non-linear methods however, especially in three dimensions, is the large computing time which is associated with the computation of the influence coefficients for every new cavity shape in the iterative process. Even though non-linear theories are more accurate, linear theories are more versatile in the design process. In addition, linear theories, especially when applied to supercavitating hydrofoils, provide a very good first approximation in the iterative process for determining the

non-linear cavity shape, thus reducing the associated computational effort (see, for example, [11] and Section 6 of this paper).

In the present work, the linearized supercavitating hydrofoil problem with leading edge cavity detachment is addressed by using the classical source and vorticity approach, previously utilized by Davies [13], Golden [14] and Persson [15]. The linearized boundary conditions are expressed in terms of singular integral equations of unknown source and vorticity distributions. Those integral equations are inverted analytically and expressions for the cavitation number, the source and vorticity distributions are given in terms of integrals of functions which depend only on the geometry of the hydrofoil and the cavity length. Those integrals are then computed numerically in an accurate and efficient manner to produce the cavity shapes and the pressure distributions for generally shaped hydrofoils.

The cavity shapes produced from the present method for some foil geometries and different flow conditions are finally compared with the cavity shapes produced from an existing non-linear potential based boundary element method.

## 2. Formulation of the problem

In this section, the linearized cavitating hydrofoil problem is formulated in terms of singular integral equations with respect to unknown vorticity and source distributions. This formulation has previously been utilized by, among others, Davies [13] and Golden [14]. The latter of those authors used numerical methods to invert the resulting integral equations and the former used analytical techniques from which, however, the final expressions for the vorticity and source distributions are still *coupled* to each other. More recently, Persson [15] inverted these integral equations in the case of a supercavitating flat plate and produced analytical expressions for the source and vorticity distributions. In the present work, the involved singular integral equations are inverted analytically in the case of general shape supercavitating hydrofoils. The cavitation number, the vorticity and source distributions are expressed in terms of integrals of quantities which depend *only* on the foil geometry and the cavity length.

Consider a supercavitating hydrofoil of chord length one, with a cavity of length $l > 1$, subject to a uniform flow $U_\infty$, as shown in Fig. 1. In this work we assume that the cavity starts at the leading edge on the suction side of the foil ($x = 0$) and at the trailing edge ($x = 1$) on the pressure side.

The corresponding cavitation number $\sigma$ is defined as:

$$\sigma = \frac{p_\infty - p_c}{\frac{\rho}{2} U_\infty^2}, \tag{1}$$

where $p_\infty$ is the ambient pressure and $p_c$ is the uniform pressure inside the cavity.

We define as $u$ and $v$ the perturbation velocities tangent and normal to the direction of the incoming flow respectively, as shown in Fig. 1. In the context of the linearized cavity theory the boundary conditions of the corresponding Hilbert problem are:

The kinematic boundary condition:

$$v^- = U_\infty \frac{d\eta_l}{dx}; \quad 0 < x < 1, \quad y = 0^- . \tag{2}$$

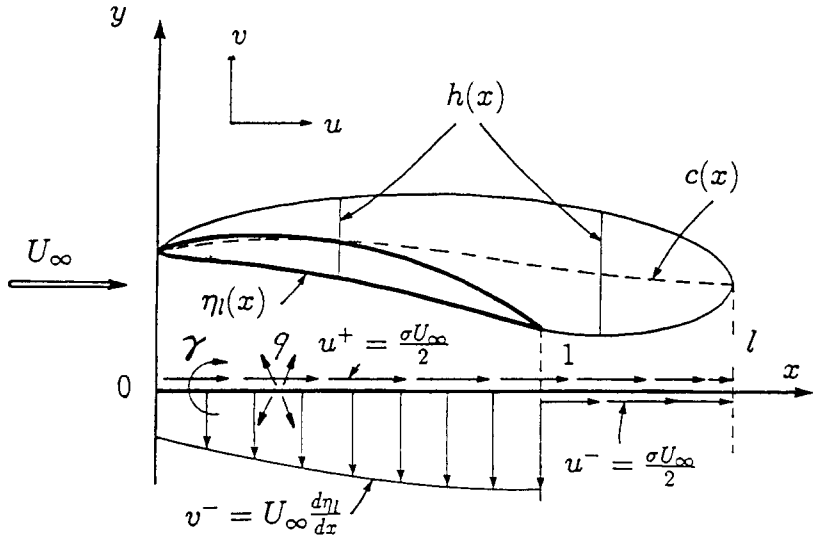


*Fig. 1.* Supercavitating hydrofoil.

The dynamic boundary conditions:

$$u^+ = \frac{\sigma}{2} U_\infty ; \quad 0 < x < 1 , \quad y = 0^+ , \tag{3}$$

$$u^- = \frac{\sigma}{2} U_\infty ; \quad 1 < x < l , \quad y = 0^- , \tag{4}$$

where $\eta_l(x)$ is the ordinate of the lower hydrofoil surface, as shown in Fig. 1. These boundary conditions can be expressed in terms of vorticity and source distributions[1] $\gamma(x)$ and $q(x)$, respectively, located on the slit $x \in [0, l]$:

$$v^- = -\frac{q}{2} + \frac{1}{2\pi} \int_0^l \frac{\gamma(\xi)\, d\xi}{\xi - x} , \tag{5}$$

$$u^+ = \frac{\gamma}{2} - \frac{1}{2\pi} \int_0^l \frac{q(\xi)\, d\xi}{\xi - x} , \tag{6}$$

$$u^- = -\frac{\gamma}{2} - \frac{1}{2\pi} \int_0^l \frac{q(\xi)\, d\xi}{\xi - x} , \tag{7}$$

By using Equations (3), (4), (6), and (7) it can easily be shown that:

$$\gamma(x) = 0 ; \quad 1 < x < l . \tag{8}$$

Finally, and with the use of the definitions:

$$\bar{\gamma}(x) = \frac{\gamma(x)}{\sigma U_\infty} \quad \text{and} \quad \bar{q}(x) = \frac{q(x)}{\sigma U_\infty} , \tag{9}$$

[1] With $\int$ designating the Cauchy principal value of the integral.

the complete boundary value problem becomes:

1. *Kinematic Boundary Condition*

$$-\frac{\bar{q}}{2}+\frac{1}{2\pi}\int_0^1 \frac{\bar{\gamma}(\xi)\,d\xi}{\xi-x}=\Theta_l^*(x)\,;\quad 0<x<1\,,\quad y=0^-\,. \tag{10}$$

2. *Dynamic Boundary Condition*

$$\frac{\bar{\gamma}}{2}-\frac{1}{2\pi}\int_0^l \frac{\bar{q}(\xi)\,d\xi}{\xi-x}=\frac{1}{2}\,;\quad 0<x<l\,,\quad y=0^+\,. \tag{11}$$

3. *Kutta Condition*

$$\bar{\gamma}(1)=0\,. \tag{12}$$

4. *Cavity Closure Condition*[2]

$$\int_0^l \bar{q}(x)\,dx=0\,, \tag{13}$$

where

$$\Theta_l^*=\frac{1}{\sigma}\frac{d\eta_l}{dx}\,. \tag{14}$$

## 3. Inversion of the integral equations

The singular integral equations of Cauchy type, (10) and (11), can be inverted to produce expressions for the unknown $\sigma$, $\bar{\gamma}(x)$ and $\bar{q}(x)$ in terms of the cavity length $l$ and the lower hydrofoil surface $\eta_l(x)$, as follows:

First, Equation (11) is inverted with respect to the unknown $\bar{q}(x)$ [17] to produce:

$$\bar{q}(x)=-\sqrt{\frac{x}{l-x}}+\frac{1}{\pi}\sqrt{\frac{x}{l-x}}\int_0^1\sqrt{\frac{l-\xi}{\xi}}\,\frac{\bar{\gamma}(\xi)\,d\xi}{x-\xi}\,, \tag{15}$$

where use of Equation (8) has been made. Notice that the expression (15) corresponds to the unique solution to (11) which behaves like $1/\sqrt{l-x}$ at the trailing edge of the cavity (Wu's singularity [18]). By substituting Equation (15) in (10) and by using the substitutions:

$$z=\sqrt{\frac{x}{l-x}}\,,\qquad \eta=\sqrt{\frac{\xi}{l-\xi}}\,,\qquad t=\sqrt{\frac{1}{l-1}}\,, \tag{16}$$

[2] We apply the linearized cavity closure condition in which the cavity is required to have zero thickness at its trailing edge. The present method can be extended to treat open cavities at the trailing edge with the openness of the cavity, possibly supplied from further knowledge of the viscous wake behind the cavity [16]. This, however, is outside the scope of this work.

we arrive at the following singular integral equation of Cauchy type for $\bar{\gamma}$:

$$\frac{1}{2\pi}\int_0^t \frac{\bar{\gamma}(\eta)\,\mathrm{d}\eta}{(1+\eta^2)(z-\eta)} = \frac{z}{4(1+z^2)} - \frac{\Theta_l^*(z)}{2(1+z^2)}\,. \tag{17}$$

Inversion of Equation (17) with respect to the variable $\bar{\gamma}(\eta)/(1+\eta^2)$ renders finally:

$$\bar{\gamma}(z) = -\frac{(1+z^2)}{\pi}\sqrt{\frac{t-z}{z}}\int_0^t \sqrt{\frac{\eta}{t-\eta}}\,\frac{\frac{\eta}{2}-\Theta_l^*(\eta)}{(1+\eta^2)(z-\eta)}\,\mathrm{d}\eta\,. \tag{18}$$

Notice that $\bar{\gamma}(z)$ in Equation (18) is the unique solution to (17) which satisfies the Kutta condition (12).

The cavitation number $\sigma$ is determined by satisfying the cavity closure condition (13). First, by substituting Equation (15) in (13) and by using Equations (8), (37) and (39) we get:

$$-\frac{\pi l}{2} + \int_0^1 \sqrt{\frac{l-\xi}{\xi}}\,\bar{\gamma}(\xi)\,\mathrm{d}\xi = 0\,, \tag{19}$$

and by applying Equations (18), (49), (43), (41) and (42) we get the following general expression for $\sigma$:

$$\sigma = \frac{4\sqrt{2}r^4}{\pi(r^2+1)}\int_0^t \sqrt{\frac{\eta}{t-\eta}}\,\frac{\sqrt{r^2+1}+\eta\sqrt{r^2-1}}{(1+\eta^2)^2}\left[-\frac{\mathrm{d}\eta_l}{\mathrm{d}x}\right]\mathrm{d}\eta\,, \tag{20}$$

where $r = \sqrt{1+t^2}$.

The source distribution is derived by substituting Equation (18) into Equation (15) and by using Equations (49), (45), (46) and (47):

$$\begin{aligned}\bar{q}(z) = {} & -\Theta_l^*(z) + \sqrt{\frac{t+z}{z}}\,\frac{(\sqrt{r^2-1}-z\sqrt{r^2+1})}{2\sqrt{2}r^2} \\ & - \frac{1+z^2}{\pi}\sqrt{\frac{t+z}{z}}\int_0^t \sqrt{\frac{\omega}{t-\omega}}\,\frac{\Theta_l^*(\omega)\,\mathrm{d}\omega}{(1+\omega^2)(z+\omega)}\end{aligned} \tag{21}$$

for $z < t$, and

$$\begin{aligned}\bar{q}(z) = {} & \sqrt{\frac{t+z}{z}}\,\frac{(\sqrt{r^2-1}-z\sqrt{r^2+1})}{2\sqrt{2}r^2} - \frac{1+z^2}{\pi}\sqrt{\frac{t+z}{z}}\int_0^t \sqrt{\frac{\omega}{t-\omega}}\,\frac{\Theta_l^*(\omega)\,\mathrm{d}\omega}{(1+\omega^2)(z+\omega)} \\ & - \sqrt{\frac{z-t}{z}}\,\frac{(z\sqrt{r^2+1}+\sqrt{r^2-1})}{2\sqrt{2}r^2} - \frac{1+z^2}{\pi}\sqrt{\frac{z-t}{z}}\int_0^t \sqrt{\frac{\omega}{t-\omega}}\,\frac{\Theta_l^*(\omega)\,\mathrm{d}\omega}{(1+\omega^2)(z-\omega)}\end{aligned} \tag{22}$$

for $z > t$.

The cavity thickness $h(x)$, which also includes the foil thickness as shown in Fig. 1, is determined, within the framework of linearized theory, by integrating the equation

$$U_\infty \frac{\mathrm{d}h}{\mathrm{d}x} = q(x)\,. \tag{23}$$

The camber of the cavity in the wake, $c(x)$, is determined by integrating the following

equation:

$$U_\infty \frac{dc}{dx} = v_w(x) \quad \text{for } 1 < x < l\,, \tag{24}$$

where $v_w(x)$ is the normal perturbation velocity in the wake, given as follows:

$$v_w(x) = -\frac{1}{2\pi}\int_0^1 \frac{\gamma(\xi)\,d\xi}{x-\xi}\,; \quad 1 < x < l\,, \quad y = 0\,. \tag{25}$$

By substituting Equation (18) in (25) and by using (49), (48), (46) and (47) we get $v_w$ in terms of the hydrofoil geometry:

$$\frac{v_w(z)}{\sigma U_\infty} = \sqrt{\frac{t+z}{z}}\,\frac{(\sqrt{r^2-1}-z\sqrt{r^2+1})}{4\sqrt{2}r^2} - \frac{1+z^2}{2\pi}\sqrt{\frac{t+z}{z}}\int_0^t \sqrt{\frac{\omega}{t-\omega}}\,\frac{\Theta_l^*(\omega)\,d\omega}{(1+\omega^2)(z+\omega)}$$
$$-\sqrt{\frac{z-t}{z}}\,\frac{(z\sqrt{r^2+1}+\sqrt{r^2-1})}{4\sqrt{2}r^2} - \frac{1+z^2}{2\pi}\sqrt{\frac{z-t}{z}}\int_0^t \sqrt{\frac{\omega}{t-\omega}}\,\frac{\Theta_l^*(\omega)\,d\omega}{(1+\omega^2)(z-\omega)}\,. \tag{26}$$

The pressure distribution on the upper and lower cavity or foil surface is given, in the context of linear theory, as follows:

$$C_p^+ = -2\sigma\left[\frac{\bar{\gamma}}{2} - \frac{1}{2\pi}\int_0^l \frac{\bar{q}(\xi)\,d\xi}{\xi - x}\right]; \quad 0 < x < l\,, \quad y = 0^+\,, \tag{27}$$

$$C_p^- = -2\sigma\left[-\frac{\bar{\gamma}}{2} - \frac{1}{2\pi}\int_0^l \frac{\bar{q}(\xi)\,d\xi}{\xi - x}\right]; \quad 0 < x < l\,, \quad y = 0^-\,, \tag{28}$$

where $C_p$ is the pressure coefficient defined as:

$$C_p = \frac{p - p_\infty}{\frac{\rho}{2}U_\infty^2}\,. \tag{29}$$

## 4. Numerical integrations

The integrals in Equations (20), (18), (21) and (22) are computed numerically with special care taken at the singularities of the integrands. We first define the transformation:

$$\eta = t\sin^2\left(\frac{\theta}{2}\right); \quad 0 \le \eta \le t \quad \text{and} \quad 0 \le \theta \le \pi\,. \tag{30}$$

Next, we express the involved integrals in terms of $\theta$, thus avoiding the square root singularities of the integrands at $\eta = 0$ and $\eta = t$. The numerical integrations are then performed by applying Simpson's rule with $K$ uniform intervals in $\theta$.

To compute the principal value of the singular integral in Equation (18), we first factor out the involved singularity as follows:

$$\int_0^t \sqrt{\frac{\eta}{t-\eta}}\,\frac{f(\eta)}{z-\eta}\,d\eta = \int_0^t \sqrt{\frac{\eta}{t-\eta}}\,\frac{f(\eta)-f(z)}{z-\eta}\,d\eta - \pi f(z)\,, \tag{31}$$

where

$$f(\eta) = \frac{\frac{\eta}{2} - \Theta_l^*(\eta)}{1 + \eta^2}$$

and Equation (39) has been used. Notice that the integrand in the integral of Equation (31) is not singular anymore, and thus the integral is computed numerically by applying the same methodology described in the beginning of this section.

To find the cavity thickness distribution, we perform the integration in Equation (23) numerically after making the transformation

$$x = l \sin^2\left(\frac{\phi}{2}\right); \quad 0 \leq x \leq l \quad \text{and} \quad 0 \leq \phi \leq \pi . \tag{32}$$

We then compute the discretized thickness distribution by using the algorithm

$$h_{i+1} = h_i + \frac{l}{2U_\infty} \int_{\phi_i}^{\phi_{i+1}} q(x) \sin \phi \, \mathrm{d}\phi ; \quad i = 1, \ldots, N \tag{33}$$

with

$$h_1 = 0 \quad \text{at } \phi_1 = 0 \tag{34}$$

and

$$\phi_{i+1} = \phi_i + \frac{\pi}{N} ; \quad i = 1, \ldots, N . \tag{35}$$

The integral in Equation (33) is computed numerically by applying Simpson's rule with one interval (i.e. three points).

The chamber distribution is determined by integrating Equation (24) numerically, using the same technique described previously for the cavity thickness distribution.

The convergence of the numerical integrations is shown in Tables 1 and 2 for a supercavitating flat plate at an angle for which analytical results exist in the literature [5]. The cavity volume shown in Table 2 has been determined by integrating the cavity thickness as computed from Equation (33). The convergence is excellent even for small numbers of Simpson's intervals and for a broad range of cavity lengths. More convergence tests for some common camber and thickness distributions can be found in [19].

*Table 1.* Flat plate at $\alpha = 1$ rad, cavitation number $\sigma$

| $l$ | Analytical | Numerical | | |
|---|---|---|---|---|
| | | $K = 20$ | $K = 10$ | $K = 5$ |
| 1.1 | 6.324555 | 6.324555 | 6.324560 | 6.329471 |
| 1.3 | 3.651484 | 3.651484 | 3.651484 | 3.651730 |
| 1.5 | 2.828427 | 2.828427 | 2.828427 | 2.828405 |
| 1.8 | 2.236068 | 2.236068 | 2.236068 | 2.236057 |
| 2.0 | 2.000000 | 2.000000 | 2.000000 | 1.999995 |

*Table 2.* Flat plate at $\alpha = 1$ rad, cavity number V

| $l$ | Analytical | Numerical | | |
|---|---|---|---|---|
| | | $K = 20$ | $K = 10$ | $K = 5$ |
| 1.1 | 1.272656 | 1.272656 | 1.272668 | 1.282604 |
| 1.3 | 1.327715 | 1.327715 | 1.327715 | 1.328218 |
| 1.5 | 1.554475 | 1.554475 | 1.554475 | 1.554295 |
| 1.8 | 1.975729 | 1.975729 | 1.975729 | 1.975635 |
| 2.0 | 2.288818 | 2.288818 | 2.288818 | 2.288768 |

## 5. Results

Results produced by applying the present method on a typical hydrofoil section are shown in Fig. 2. The pressure distribution shown in Fig. 2 is determined by integrating numerically Equations (27) and (28) by using techniques similar to those described in Section 4. Note that the pressure coefficient, $C_p$, is constant everywhere on the cavity and equal to the negative of the cavitation number $\sigma = 0.281$. This provides a very good validation test on the involved expressions as well as on the related numerical integrations.

Finally, cavity shapes predicted by applying the present linearized method and a non-linear boundary element method [12] are shown in Figs 3 to 7 for a parabolic camber section at different angles of attack and different cavity lengths. As expected, the differences between cavity shapes from linear and non-linear theory become larger for larger angles of attack and for shorter cavities.

The boundary element method is described in detail in [12]. It consists a perturbation potential based boundary element method. The foil and cavity are panelled with constant strength dipole and source panels. The strength of the dipoles is proportional to the potential at each panel and is known on the cavity, due to the dynamic boundary condition, but is unknown on the fully wetted panels. The strength of the sources, on the other hand, is

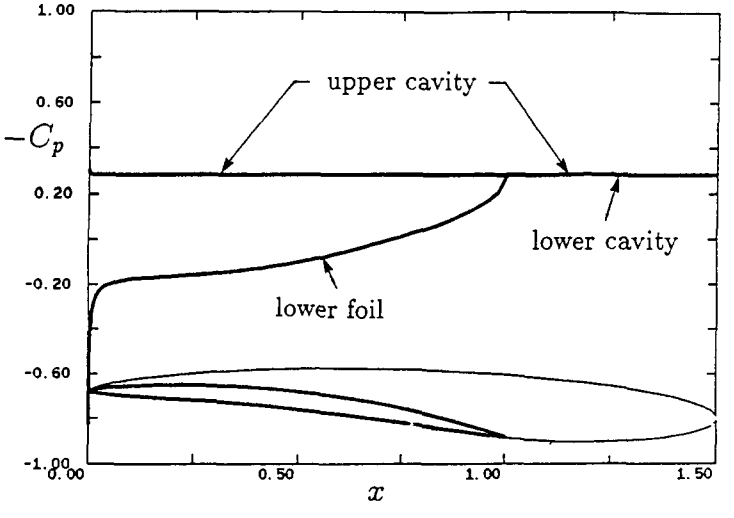


*Fig. 2.* Cavity shape and pressure distributions as predicted from the present method. NACA16-004 thickness section with parabolic camber with maximum camber to chord ratio 3%, at an angle of attack $\alpha = 5°$. Cavity length $l = 1.5$. Predicted cavitation number $\sigma = 0.281$.

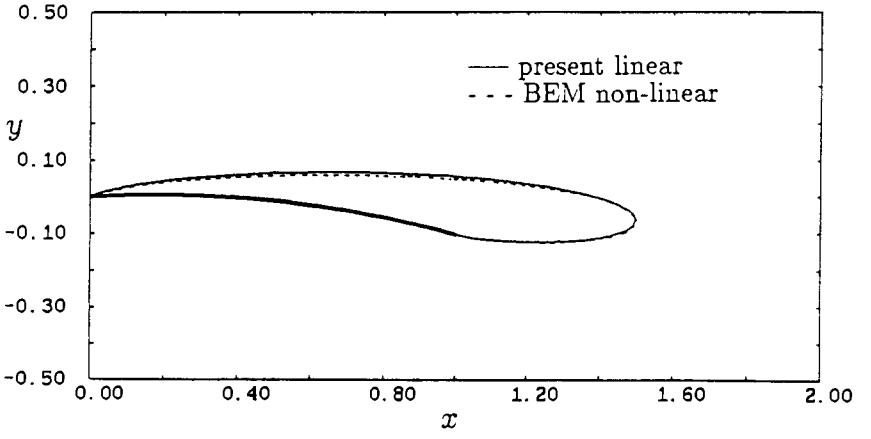


*Fig. 3.* Cavity shapes predicted by applying the present method and the boundary element method by Kinnas & Fine (1990). Parabolic camber with maximum camber to chord ratio 4%. Angle of attack $\alpha = 6°$. Cavity length $l = 1.5$.

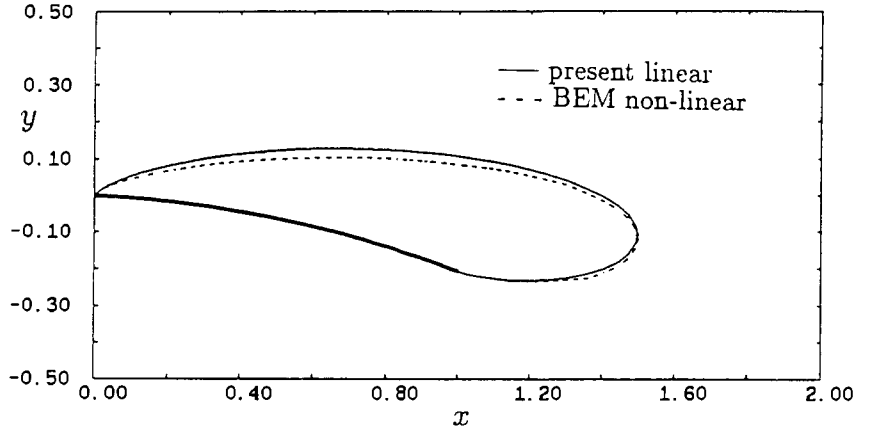


*Fig. 4.* Cavity shapes predicted by applying the present method and the boundary element method by Kinnas & Fine (1990). Parabolic camber with maximum camber to chord ratio 4%. Angle of attack $\alpha = 12°$. Cavity length $l = 1.5$.

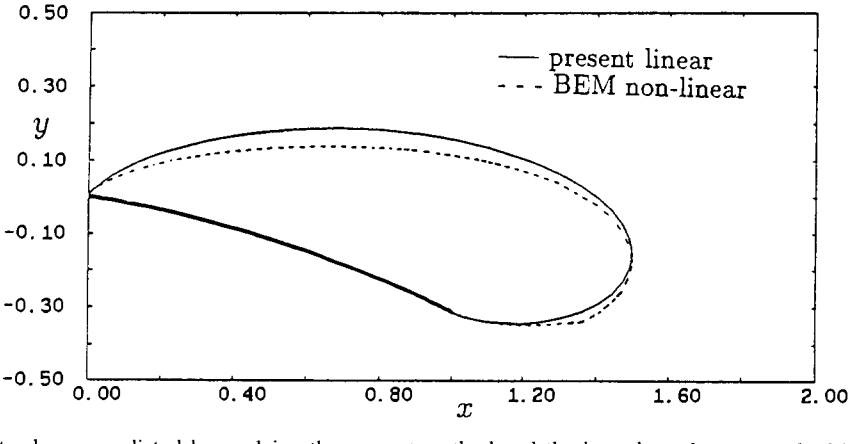


*Fig. 5.* Cavity shapes predicted by applying the present method and the boundary element method by Kinnas & Fine (1990). Parabolic camber with maximum camber to chord ratio 4%. Angle of attack $\alpha = 18°$. Cavity length $l = 1.5$.

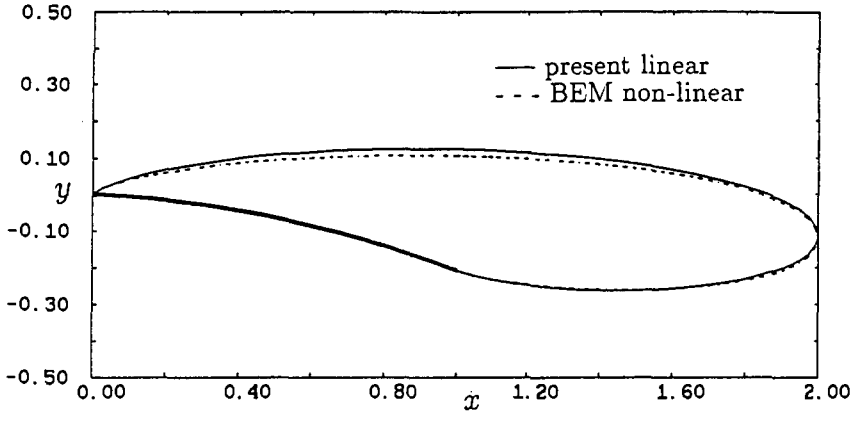


*Fig. 6.* Cavity shapes predicted by applying the present method and the boundary element method by Kinnas & Fine (1990). Parabolic camber with maximum camber to chord ratio 4%. Angle of attack $\alpha = 12°$. Cavity length $l = 2.0$.

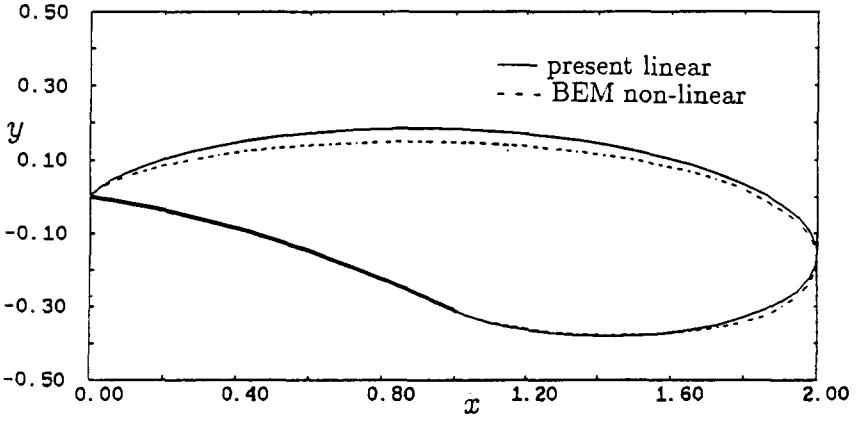


*Fig. 7.* Cavity shapes predicted by applying the present method and the boundary element method by Kinnas & Fine (1990). Parabolic camber with maximum camber to chord ratio 4%. Angle of attack $\alpha = 18°$. Cavity length $l = 2.0$.

known on the fully wetted part of the foil, due to the kinematic boundary condition, but unknown on the cavity. The unknowns (including the corresponding cavitation number) are determined by applying Green's formula for the perturbation potential at the midpoints of all panels. The shape of the cavity is determined iteratively with the first iteration being that from linear theory. It has been found that the cavity shape coverages quickly (typically in one to two iterations).

## 6. Conclusions

The supercavitating hydrofoil with leading edge cavity detachment problem was treated in linear theory by employing a source and vorticity formulation. The related integral equations were inverted analytically and the cavitation number, the source and vorticity distributions were expressed in terms of integrals of quantities which depend only on the hydrofoil geometry. These integrals were then computed numerically in a very accurate as well as

efficient way. The cavity shapes and the corresponding pressure distributions were also computed via integrations of known quantities.

The derived analytic expressions for the source and vorticity expressions are useful in validating the results from numerical methods based on the discrete vortex and source formulation [20]. Such a formulation has been utilized in predicting unsteady propeller sheet cavitation, a method originally developed by C-S. Lee [21] and recently improved by Kerwin and Kinnas [22].

## Appendix

*List of integrals*

In this Appendix a list of integrals used throughout our analysis is given, along with some instructions for their derivation. The following integrals (37) to (39) have been evaluated by using the transformation:

$$x = l\sin^2\left(\frac{\theta}{2}\right) \quad \text{or} \quad z = t\sin^2\left(\frac{\theta}{2}\right); \quad 0 \leq \theta \leq \pi, \tag{36}$$

$$\int_0^l \sqrt{\frac{x}{l-x}}\,\mathrm{d}x = \frac{\pi l}{2}, \tag{37}$$

$$\int_0^l x\sqrt{\frac{x}{l-x}}\,\mathrm{d}x = \frac{3\pi l^2}{8}, \tag{38}$$

$$\fint_0^t \sqrt{\frac{z}{t-z}}\,\frac{1}{\eta - z}\,\mathrm{d}z = -\pi; \qquad 0 \leq \eta \leq t,$$

$$= \pi\sqrt{\frac{\eta}{\eta - t}} - \pi; \quad \eta > t. \tag{39}$$

The next integrals (40) to (42) have been taken from [15] where they have been evaluated by straightforward application of the calculus of residues ($r = \sqrt{1+s^2}$).

$$\int_0^s \sqrt{\frac{z}{s-z}}\,\frac{1}{(1+z^2)^2}\,\mathrm{d}z = \frac{\pi}{4\sqrt{2}}\,\frac{s(s^2+3)\sqrt{r^2+1} - 2\sqrt{r^2-1}}{r^8}, \tag{40}$$

$$\int_0^s \sqrt{\frac{z}{s-z}}\,\frac{z}{(1+z^2)^2}\,\mathrm{d}z = \frac{\pi}{4\sqrt{2}}\,\frac{2s^2\sqrt{r^2+1} + s(s^2-1)\sqrt{r^2-1}}{r^8}, \tag{41}$$

$$\int_0^s \sqrt{\frac{z}{s-z}}\,\frac{z^2}{(1+z^2)^2}\,\mathrm{d}z = \frac{\pi}{4\sqrt{2}}\,\frac{s(3s^2-1)\sqrt{r^2+1} - (4s^2+2)\sqrt{r^2-1}}{r^8}. \tag{42}$$

The next integrals have been evaluated by breaking the integrand into partial fractions and then by evaluating each of the corresponding integral individually ($r = \sqrt{1+t^2}$):

$$\fint_0^t \sqrt{\frac{t-z}{z}}\,\frac{1}{1+z^2}\,\frac{1}{z-\eta}\,\mathrm{d}z = -\frac{\pi}{\sqrt{2}(1+\eta^2)}\left(\sqrt{r^2+1} + \eta\sqrt{r^2+1}\right). \tag{43}$$

Define:

$$R(\omega, z) = \int_0^t \sqrt{\frac{t-\eta}{\eta}} \frac{1}{z^2-\eta^2} \frac{1}{\eta-\omega} \, d\eta \,, \tag{44}$$

then:

$$R(\omega, z) = \frac{\pi}{2z(z+\omega)} \sqrt{\frac{t+z}{z}} \;; \quad 0 \leq z \leq t \,,$$

$$= \frac{\pi}{2z(z+\omega)} \sqrt{\frac{t+z}{z}} - \frac{\pi}{2z(z-\omega)} \sqrt{\frac{z-t}{z}} \;; \quad z > t \,, \tag{45}$$

$$\int_0^t \sqrt{\frac{\omega}{t-\omega}} \frac{1}{1+\omega^2} \frac{\omega}{z+\omega} \, d\omega = \frac{1}{1+z^2} \frac{\pi}{\sqrt{2}r^2} (\sqrt{r^2-1} - z\sqrt{r^2+1}) + \pi \sqrt{\frac{z}{z+t}} \frac{z}{1+z^2} \,, \tag{46}$$

$$\int_0^t \sqrt{\frac{\omega}{t-\omega}} \frac{1}{1+\omega^2} \frac{\omega}{z-\omega} \, d\omega = -\frac{1}{1+z^2} \frac{\pi}{\sqrt{2}r^2} (z\sqrt{r^2+1} + \sqrt{r^2-1})$$

$$+ \pi \sqrt{\frac{z}{z-t}} \frac{z}{1+z^2} \;; \quad z > t \,, \tag{47}$$

$$\int_0^t \sqrt{\frac{t-\eta}{\eta}} \frac{\eta \, d\eta}{(z^2-\eta^2)(\eta-\omega)} = \frac{\pi}{2} \left[ \frac{1}{z+\omega} \sqrt{\frac{t+z}{z}} - \frac{1}{z-\omega} \sqrt{\frac{z-t}{z}} \right] \;; \quad z \geq t \,, \tag{48}$$

Finally, in order to change the order of integration in a double integral, we use the Poincaré–Bertrand formula [17]:

$$\int_a^b \frac{dx}{x-x_0} \int_a^b \frac{f(x, x_1)}{x_1 - x} \, dx_1 = -\pi^2 f(x_0, x_0) + \int_a^b dx_1 \int_a^b \frac{f(x, x_1)}{(x-x_0)(x_1-x)} \, dx \,. \tag{49}$$

**Acknowledgements**

This research was sponsored by the General Hydromechanics Research Program of the U.S. Navy, Contract N00014-84-0067, and by the Applied Hydromechanics Research Program administered by the Office of Naval Research, Contract N00014-90-J-1086. The author would like to thank Mr Neal E. Fine, a doctoral student in the Department of Ocean Engineering, for his help with the computer codes.

**References**

1. M.P. Tulin, *Steady Two-Dimensional Cavity Flows About Slender Bodies*. Technical Report 834, DTMB, May 1953.
2. M.P. Tulin and M.P. Burkart, *Linearized Theory for Flows About Lifting Foils at Zero Cavitation Number*. Technical Report C-638, DTMB, February 1955.
3. M.P. Tulin, Supercavitating flow past foils and struts. In *Symposium on Cavitation in Hydrodynamics*, NPL, Tenddington, England, September 1955.
4. T.Y. Wu, *A Note on the Linear and Nonlinear Theories for Fully Cavitated Hydrofoils*. Technical Report No. 21-22, California Institute of Technology, Hydrodynamics Laboratory, August 1956.

5. J.A. Geurst, Linearized theory for fully cavitated hydrofoils. *International Shipbuilding Progress* 7(65), January 1960.
6. B.R. Parkin, *Munk Integrals for Fully Cavitated Hydrofoils*. Technical Report P-2350-1, RAND, November 1961.
7. A.G. Fabula, Thin-airfoil theory applied to hydrofoils with a single finite cavity and arbitrary free streamline detachment. *Journal of Fluid Mechanics* 12 (1962) 227–240.
8. Nishiyama T. and Ota T, Linearized potential flow models for hydrofoils in supercavitating flows. *Transactions of the ASME*, December 1971.
9. T. Hanaoka, Linearized theory of cavity flow past a hydrofoil of arbitrary shape. *Journal of the Society of Naval Architects, Japan* 115 (1964) 56–74.
10. C. Pellone and A. Rowe, Supercavitating hydrofoils in non-linear theory. In: *Third International Conference on Numerical Ship Hydrodynamics*, Basin d'essais des Carènes, Paris, France, June 1981.
11. J.S. Uhlman, The surface singularity or boundary integral method applied to supercavitating hydrofoils. *Journal of Ship Research* 33(1) (1989) 16–20.
12. S.A. Kinnas and N.E. Fine, Non-linear analysis of the flow around partially or super-cavitating hydrofoils by a potential based panel method. In: Morino and Piva (eds), *Boundary Integral Methods - Theory and Applications*. Proceedings of the IABEM-90 Symposium, Rome, October 1990. Springer-Verlag.
13. T.V. Davies, Steady two-dimensional cavity flow past an aerofoil using linearized theory. *Quart. Journ. Mech. and Applied Math.* XXIII (Pt. I) (1970) 49–76.
14. D.W. Golden, *A Numerical Method for Two-dimensional, Cavitating, Lifting Flows*. Master's thesis, Department of Ocean Engineering, MIT, May 1975.
15. B. Persson, *Theoretical Study of Cavitation on Flat Plate*. Technical Report 78/440, DnV, 1978.
16. H. Yamaguchi and H. Kato, On application on non-linear cavity flow theory to thick foil sections. In *Second Conference on Cavitation*, Institution of Mechanical Engineers, Edinburgh, September 1983.
17. N.I. Muskhelishvili, *Singular Integral Equations*. Groningen: Noordhoff (1953) 447 pp.
18. T.Y. Wu, *A Simple Method for Calculating the Drag in the Linear Theory of Cavity Flows*. Technical Report No. 85-5, California Institute of Technology, Hydrodynamics Laboratory, August 1957.
19. S.A. Kinnas, *Cavity Shape Characteristics for Supercavitating Hydrofoils*. Technical Report 84-13, MIT, Department of Ocean Engineering, October 1984.
20. N.E. Fine, *Computational and Experimental Investigations of the Flow Around Cavitating Hydrofoils*. Technical Report No. 88-6, MIT, Department of Ocean Engineering, September 1988.
21. Chung-Sup Lee, *Prediction of Steady and Unsteady Performance of Marine Propellers with or without Cavitation by Numerical Lifting Surface Theory*. PhD thesis, M.I.T., Department of Ocean Engineering, May 1979.
22. J.E. Kerwin, S.A. Kinnas, M.B. Wilson and J. McHugh, Experimental and analytical techniques for the study of unsteady propeller sheet cavitation. In: *Proceedings of the Sixteenth Symposium on Naval Hydrodynamics*, Berkeley, California, July 1986.